Three-dimensional simulations of two-fluid drift-Braginskii turbulence

A. Zeiler, J. Bowman, D. Biskamp
Max-Planck-Institut für Plasmaphysik, EURATOM Association
85748 Garching, Germany

1. Introduction

A physics-based understanding and prediction of plasma-edge confinement requires the investigation of the complete two-fluid drift-Braginskii equations [1] in realistic geometry. In this paper we extend previous approaches (see Refs. [2,3] and citations within) in two ways. *(a)* Ion temperature dynamics are self-consistently taken into account. This allows us to study, within the same system, turbulence driven by resistive modes, which was previously treated in the cold ion limit, and η_i-mode turbulence. It also enables us to check whether the nonadiabatic electron response at the plasma-edge modifies the η_i-mode, since resistive effects usually are neglected in simulations of η_i-mode turbulence (see e.g. Refs. [4-6]). *(b)* To account for the fully nonlinear self-consistent evolution of the plasma-edge profile and to make efficient use of parallel computers with distributed memory architecture, we have developed and applied an anisotropic multrigrid Poisson solver to simulate resistive drift-wave turbulence in sheared magnetic geometry.

2. Ion temperature fluctuations

Our investigations of ion temperature effects are based on the electrostatic drift-Braginskii equations [1] in a flux-tube domain with field-aligned coordinates [3],

$$\nabla_\perp \cdot \frac{d}{dt}\nabla_\perp(\phi + \tau\alpha p_i) + \hat{C}\frac{p_e + \tau p_i}{1+\tau} + \frac{\partial^2 h}{\partial z^2} = 0, \tag{1a}$$

$$\frac{dn}{dt} + \frac{\partial\phi}{\partial y} - \left[\epsilon_n \hat{C}(\phi - \alpha p_e) - \alpha\epsilon_n(1+\tau)\frac{\partial^2 h}{\partial z^2}\right] = 0, \tag{1b}$$

$$\frac{dT_e}{dt} + \eta_e\frac{\partial\phi}{\partial y} - \frac{2}{3}\left[\epsilon_n\hat{C}(\phi - \alpha p_e) - 1.71\alpha\epsilon_n(1+\tau)\frac{\partial^2 h}{\partial z^2} + \kappa_\parallel\frac{\partial^2 T_e}{\partial z^2}\right] = 0, \tag{1c}$$

$$\frac{dT_i}{dt} + \eta_i\frac{\partial\phi}{\partial y} - \frac{2}{3}\left[\epsilon_n\hat{C}(\phi - \alpha p_e) - \alpha\epsilon_n(1+\tau)\frac{\partial^2 h}{\partial z^2}\right] = 0, \tag{1d}$$

with $p_e = n + T_e$, $p_i = n + T_i$, $h = \phi - \alpha(p_e + 0.71T_e)$, and $\nabla_\perp^2$, the total time derivative d/dt, and the curvature operator $\hat{C}$ defined as in [3]. The time and space units

$$t_0 = \left(\frac{RL_n}{2}\right)^{1/2}\frac{1}{c_s}, \quad L_\perp = 2\pi q_a\left(\frac{\nu_{ei}R\rho_s}{2\omega_{ce}}\right)^{1/2}\left(\frac{2R}{L_n}\right)^{1/4}, \quad L_z = 2\pi q_a R,$$

chosen to balance the three terms in Eq. (1a), are the natural choice for the resistive ballooning mode (but not for the η_i-mode which scales like ρ_s, as we will show). This normalization yields the dimensionless parameters $\alpha = (\rho_s c_s t_0)/[(1+\tau)L_n L_\perp]$, $\epsilon_n = 2L_n/R$,

$\tau = T_{i0}/T_{e0}$, $\kappa_\| = 1.6\alpha^2\epsilon_n(1+\tau)$, $\eta_e = L_n/L_{T_e}$, $\eta_i = L_n/L_{T_i}$ with $c_s^2 = (T_{e0}+T_{i0})/m_i$, $\rho_s = c_s/\omega_{ci}$, the profile e-folding lengths L_n, L_{T_e}, and L_{T_i}, and the magnetic shear parameter $\hat{s}$.

To calculate the linear properties of resistive ballooning and toroidal η_i-modes we drop the electron temperature fluctuations and Fourier-transform Eqs. (1a), (1b), (1d) in x and y keeping only the modes with $k_x = 0$. Along the magnetic field we expand in the orthogonal functions $\psi_n(z) = \exp\{-(\lambda z)^2/2\}H_n(\lambda z)$ where H_n are the Hermite polynomials. This leads to a generalized matrix eigenvalue problem for the growth rate γ, which we solve by standard numerical techniques.

We perform the eigenvalue calculations in the range of typical edge parameters $\alpha \sim 1$, $\epsilon_n \sim 0.05$, $\eta_i \sim 1$, $\hat{s} = 1$. Three main results are obtained: First, the resistive ballooning and the curvature driven η_i-mode appear as two different branches at comparable wavelengths, depending on the parameters. Second, the η_i-mode is unaffected by the non-adiabatic electron response. Its growth rate agrees surprisingly well with the one obtained without parallel resistivity. Third, the ion pressure gradient strongly supports the resistive ballooning mode. Consistent with Ref. [7] the resistive ballooning mode has a wavelength which scales like $L_\perp$ and is restricted to the low-α regime ($\alpha \leq 0.5$) by electron and ion diamagnetic effects. The η_i-mode is compared to the adiabatic limit ($\phi = \alpha n$) where the dispersion relation can be solved analytically. The analytic solution matches the numerical result obtained for arbitrary resistivity. The analytic solution allows us to show that unstable roots exist if and only if $\eta_i > 2/3$. Furthermore, we obtain the approximate scaling for the spectrum of unstable modes $k_y^2\rho_s^2 \sim 1/[\tau(\eta - 2/3)]$. This shows that η_i needs to be sufficiently larger than 2/3 to destabilize the mode in the transport relevant long wavelength regime. The characteristic wavelength of the η_i-mode scales like ρ_s, in contrast to the $L_\perp$-scaling of the resistive ballooning mode. Thus, we conclude that the relative importance of resistive ballooning and η_i-modes is largely controlled by the ratio of the two scale lengths $\rho_s/L_\perp = \alpha(1+\tau)\epsilon_n^{1/2}$ and by the parameter η_i, since steepening the temperature gradient boosts the η_i-mode due to an increased growth rate at larger wavelength.

In order to check the relevance of the linear results we proceed to direct numerical simulation of the complete set of nonlinear equations (1) using the numerical methods described in Ref. [3]. In the low-α regime the ratio $\rho_s/L_\perp = \alpha(1+\tau)\epsilon_n^{1/2}$ is always small for realistic values of ϵ_n, hence we do not expect the η_i-mode to contribute unless $\eta_i \gg 1$; this result is confirmed by the numerical simulations. In the high-α regime ($\alpha = 1.25$), where the resistive ballooning mode is stable, the η_i-mode can become important for realistic values of ϵ_n. At $\epsilon_n = 0.2$, corresponding to large $\rho_s/L_\perp$, the transport rates are high and strongly peaked at the torus outside, demonstrating the importance of the toroidal η_i-mode. Consequently the turbulence level is strongly altered if η_i is changed. If ϵ_n is reduced ($\epsilon_n = 0.1$), the ratio $\rho_s/L_\perp$ becomes smaller and the transport coefficients are lower until, at $\epsilon_n = 0.05$, the transition to nonlinearly driven drift-wave turbulence occurs (*cf.* Ref. [3] and citations within). A further reduction to $\epsilon_n = 0.02$ again strongly drives the transport. In this regime the inside/outside asymmetry is weak, reflecting the fact that the nonlinear drive does not depend on toroidicity.

3. Anisotropic multigrid Poisson solver

We have developed an object-oriented three-dimensional anisotropic multi-grid Poisson solver for simulating nonlocal collisional electrostatic drift-wave turbulence. In the design of this solver considerable effort was made to ensure that the presence of anisotropy (eg., arising from magnetic shear) does not lead to a significant degradation in performance. A three-dimensional slab version of the solver, which can be readily extended to more realistic geometries, has already been implemented for the Hasegawa–Wakatani equations. The code has been designed in a manner so that the complete nonlinear reduced Braginskii equations (*cf.* Sec. 2), including ion thermal dynamics, can be readily incorporated.

For nonlocal simulations of resistive drift-wave turbulence, we normalize (x, y, z, t) to $(\rho_s, \rho_s, L_\|, \Omega_i^{-1})$ and the total fields (ϕ, n) to $(T_e/e, \bar{n})$. Here $\rho_s = c_s/\Omega_i$, $\Omega_i = eB/(m_i c)$, $c_s = (T_e/m_i)^{1/2}$, T_e is the electron temperature, m_i is the ion mass, $L_\| = \rho_s[B/(ec\eta_\|\bar{n})]^{1/2}$, and $\bar{n}$ is some characteristic density. In this normalization, the coupled set of equations for the potential and density studied by Hasegawa and Wakatani (Ref. [8]) appear as

$$\nabla_\perp \cdot \left(n \frac{d}{dt} \nabla_\perp \phi\right) + \nabla_\| \cdot \left(\nabla_\| \phi - \frac{\nabla_\| n}{n}\right) = D_\phi {\nabla_\perp}^8 \phi, \tag{2a}$$

$$\frac{dn}{dt} + \nabla_\| \cdot \left(\nabla_\| \phi - \frac{\nabla_\| n}{n}\right) = D_n {\nabla_\perp}^6 n. \tag{2b}$$

In terms of the shear scale length L_s one may express

$$\nabla_\perp = \left(\frac{\partial}{\partial x} + z\frac{L_\|}{L_s}\frac{\partial}{\partial y}\right)\hat{x} + \frac{\partial}{\partial y}\hat{y}, \qquad \frac{d}{dt} = \frac{\partial}{\partial t} + \hat{z} \times \nabla\phi \cdot \nabla. \tag{3}$$

The hyperviscosity coefficients D_ϕ and D_n are chosen to minimize the range of scales devoted to modelling small-scale dissipation.

The coupled equations (2) are solved as an initial value problem, using a second-order predictor-corrector scheme. To avoid unnecessary restriction of the time step by the parallel-gradient terms, we treat these terms implicitly with a second-order trapezoidal approximation. At the i^{th} time step, this requires the inversion of an anisotropic elliptic operator of the form

$$\nabla_\perp \cdot (n_{i-1} \nabla_\perp \phi_i) + \frac{\Delta t}{2} \nabla_\| \cdot \left(\nabla_\| \phi_i - \frac{\nabla_\| n_i}{n_{i-1}}\right) = f_i^\phi, \tag{4a}$$

$$n_i + \frac{\Delta t}{2} \nabla_\| \cdot \left(\nabla_\| \phi_i - \frac{\nabla_\| n_i}{n_{i-1}}\right) = f_i^n; \tag{4b}$$

The advective nonlinearities, treated explicitly, are incorporated into the right-hand side. The resulting operator, linear in n_i and ϕ_i, is inverted with an anisotropic multigrid solver.

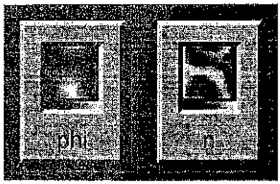

Figure 1: Typical xy-cross section of ϕ and n in the absence of magnetic shear.

This solver, which is based on an xy-zebra-surface Gauss-Seidel smoother, in turn requires the solution of

$$\nabla_\perp \cdot (n_{i-1} \nabla_\perp \phi_i) = f_i. \tag{5}$$

Solutions to this 2D anisotropic Poisson equation are obtained with a secondary multigrid solver based on an y-zebra-line Gauss-Seidel tridiagonal smoother (*cf.* Ref. [9]).

Our algorithm has distinct advantages relative to a pseudospectral Poisson solver. On a scalar machine, the computation time for our anisotropic multigrid solver is comparable to that of a pseudospectral code. However, a multi-grid solver parallelizes much more effectively over a distributed memory architecture (a parallel version of the code is currently being developed for a Cray T3E computer). A multigrid algorithm also allows the use of more general boundary conditions. Furthermore, all nonlinear terms can be retained in a straightforward manner; in contrast, pseudospectral solvers require linearization of the n_{i-1} factor appearing in (5). While the execution time for a single step of our semi-implicit algorithm is not substantially greater than that for an explicit code (based on a 2D Poisson solver), we have found that the implicit treatment of the parallel-gradient terms typically permits a time step of about four times larger. In Fig. 1 we illustrate a typical turbulent state obtained with our multigrid solver.

References

[1] A. Zeiler, J. F. Drake, B. Rogers, "Nonlinear reduced Braginskii equations with ion thermal dynamics in toroidal plasma", Phys. Plasmas, in press (1997).

[2] B. Scott, Plasma Phys. Control. Fusion **39**, 471 (1997).

[3] A. Zeiler, J. F. Drake, D. Biskamp, Phys. Plasmas **4**, 991 (1997).

[4] R. E. Waltz, Phys. Fluids **31**, 1962 (1988).

[5] M. Ottaviani, *et al.*, Phys. Fluids B **2**, 67 (1990).

[6] H. Nordman, J. Weiland, Nuclear Fusion **29**, 251 (1989).

[7] S. V. Novakovskii, *et al.*, Phys. Plasmas **2**, 781 (1995).

[8] A. Hasegawa and M. Wakatani, Phys. Rev. Lett. **50**, 682 (1983).

[9] W. Hackbusch, Multi-Grid Methods and Applications, Springer (1985).